EGU General Assembly 2022

Vienna, Austria & Online | 23–27 May 2022

EGU European Geosciences Union

Machine learning and geomorphometrical objects for convex and concave geomorphological features detection

Mihai NICULIȚĂ

Departament of Geography, Faculty of Geography and Geology,

Alexandru Ioan Cuza University of Iași, mihai.niculita@uaic.ro

Introduction

- Concave and convex features are characterizing many landforms and can be relatively easy identified by means of geomorphometric approaches. Despite this, the particularities of the landform development process and the evolution after the process cessation introduce slight changes of shape from the pure concave of convex shape. Very often this includes the apparition of compound shapes, so beside the concave or convex shape a planar or a mixture of concave and convex shape appear at the border of the landform.
- I present the case of burial mounds and sinkholes. So, despite the morphological convergence (same shape but different process), the shape particularities are influenced by the erosional process and by the later evolution of the landform. These particularities will influence mainly the precision of the concave part delineation, which is better for pure concave form and worse for deformed concavity. In the same, the particularities will allow the usage of a machine learning algorithm to learn these patterns and to be used to predict the presence of such features from the candidates in a certain area.

Segment(Object)-based Classification

- In the OBIA (Object Based Image Analysis) literature there was clearly shown that object (superpixels, segments) are better candidates for performing land-cover classifications.
- For DEMs this should be also true (Stepinski et al., 2007).
- In multiscale situations the objects delineation might need a scalar approach, but in the case of specific “simple” shapes the approach is straightforward.
- The limitations of object-based approaches are given by the over- or under-segmentation, so an assessment of these aspects is needed when using segments for classifications.

Burial mounds (kurgan, tumuli)

convex features
anthropogenic
5 m LiDAR DEM

Study area

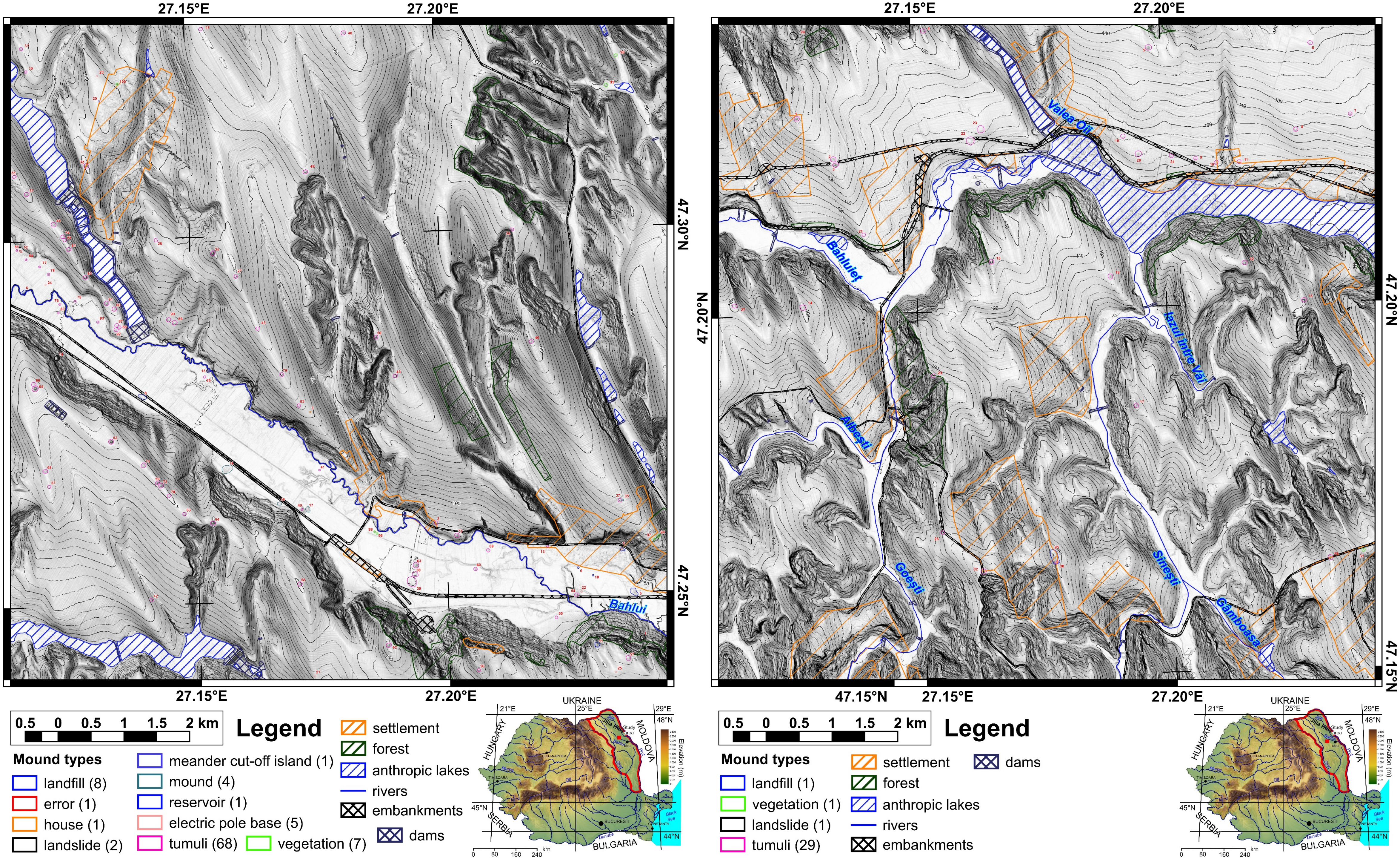
27.15°E
27.20°E
47.30°N
47.25°N
47.20°N
47.15°N
Bahlui
Bahluieț
Valea Oii
Iazul între Văi
Albești
Goești
Sinești
Gâmboașa
0.5 0 0.5 1 1.5 2 km
Legend
Mound types
landfill (8)
error (1)
house (1)
landslide (2)
meander cut-off island (1)
mound (4)
reservoir (1)
electric pole base (5)
tumuli (68)
vegetation (7)
settlement
forest
anthropic lakes
rivers
embankments
dams
landfill (1)
vegetation (1)
landslide (1)
tumuli (29)
UKRAINE
HUNGARY
MOLDOVA
SERBIA
BULGARIA
Jijia Hills
Study area
Black Sea
Danube
BUCUREȘTI
CLUJ-NAPOCA
CONSTANȚA
Elevation (m)
21°E
25°E
29°E
48°N
45°N
44°N
0 80 160 240 km

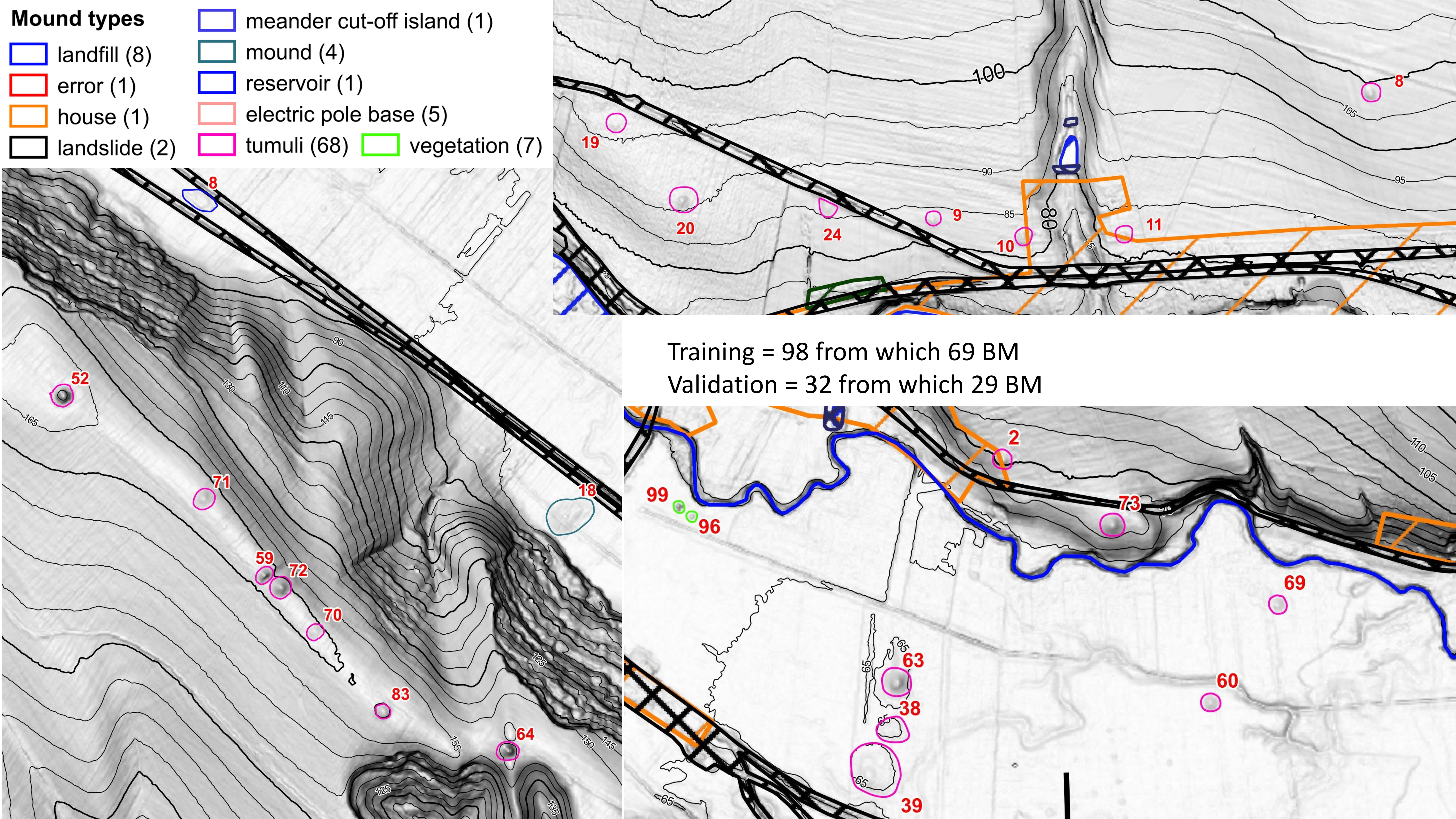

Mound types
landfill (8)
error (1)
house (1)
landslide (2)
meander cut-off island (1)
mound (4)
reservoir (1)
electric pole base (5)
tumuli (68)
vegetation (7)
Training = 98 from which 69 BM
Validation = 32 from which 29 BM
8
52
71
59
72
70
83
64
18
19
20
24
9
10
11
2
73
99
96
69
63
38
39
60


a
45
50
b
45
50
34
c
54
22
d
73
e
13
f
69
60
39
73
g
58
64
72
59
71
52
17
40
18
50
NW
SE
BM
x3
45
N
S
BM
x7.5
34
NW
SE
BM
x3
54
electric pole base
22
S
N
BM
x10
13
N
S
BM
x3
73
W
E
BM
x5
63
38
39
N
S
x10
2D
5 m
5 m
mound
segment
peak
selected peak
seed
60
S
S
BM
x10
69
W
E
BM
x10
m a.s.l.

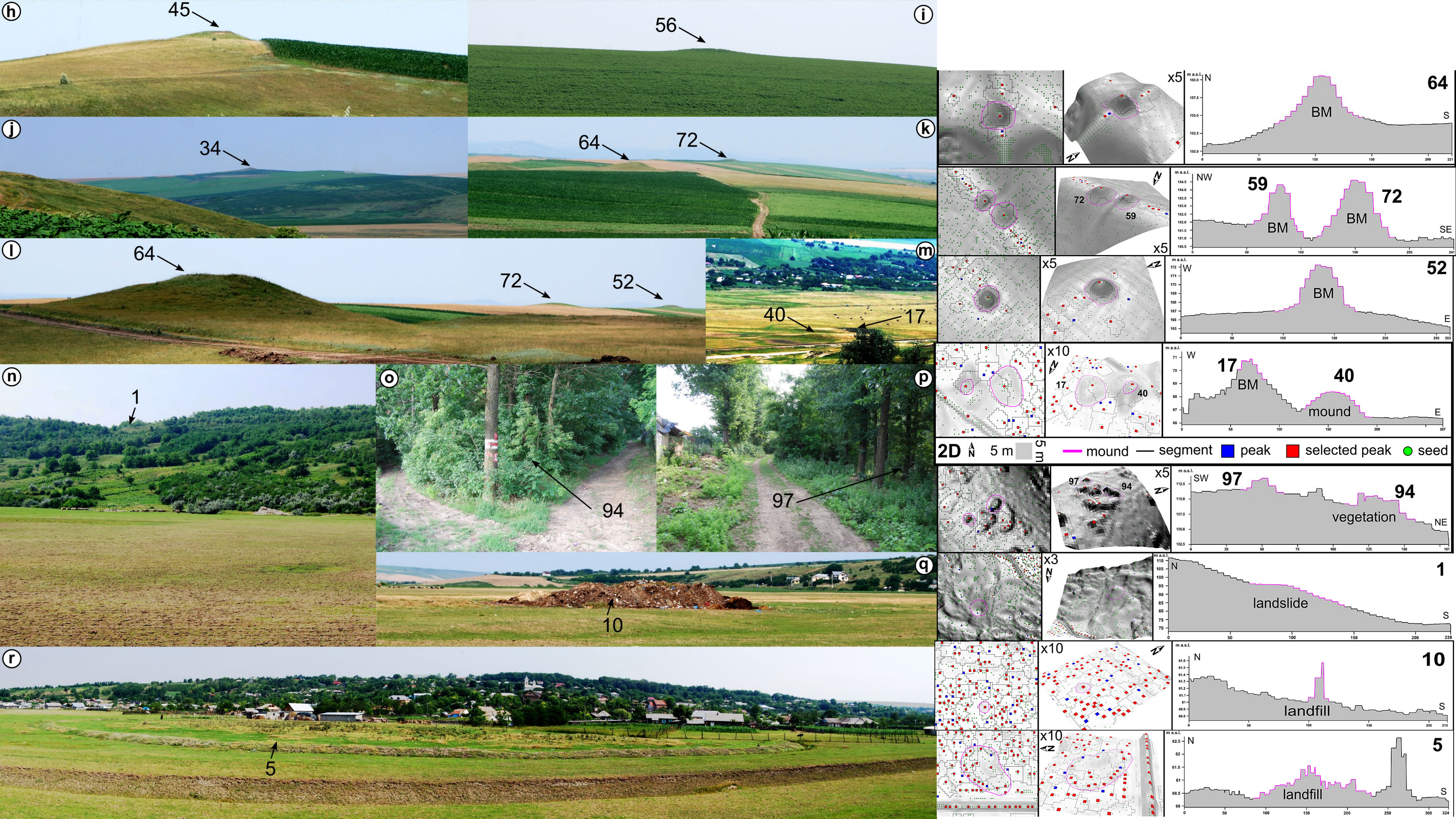
h
45
i
56
j
34
k
64
72
l
64
72
52
m
40
17
n
1
o
94
p
97
q
10
r
5
x5
N
64
BM
S
NW
59
72
BM
BM
SE
72
59
x5
x5
52
W
BM
E
x10
17
40
W
17
BM
40
mound
E
2D
5 m
5 m
mound
segment
peak
selected peak
seed
97
94
x5
SW
97
94
vegetation
NE
x3
N
1
N
landslide
S
x10
N
10
landfill
S
x10
N
5
landfill
S

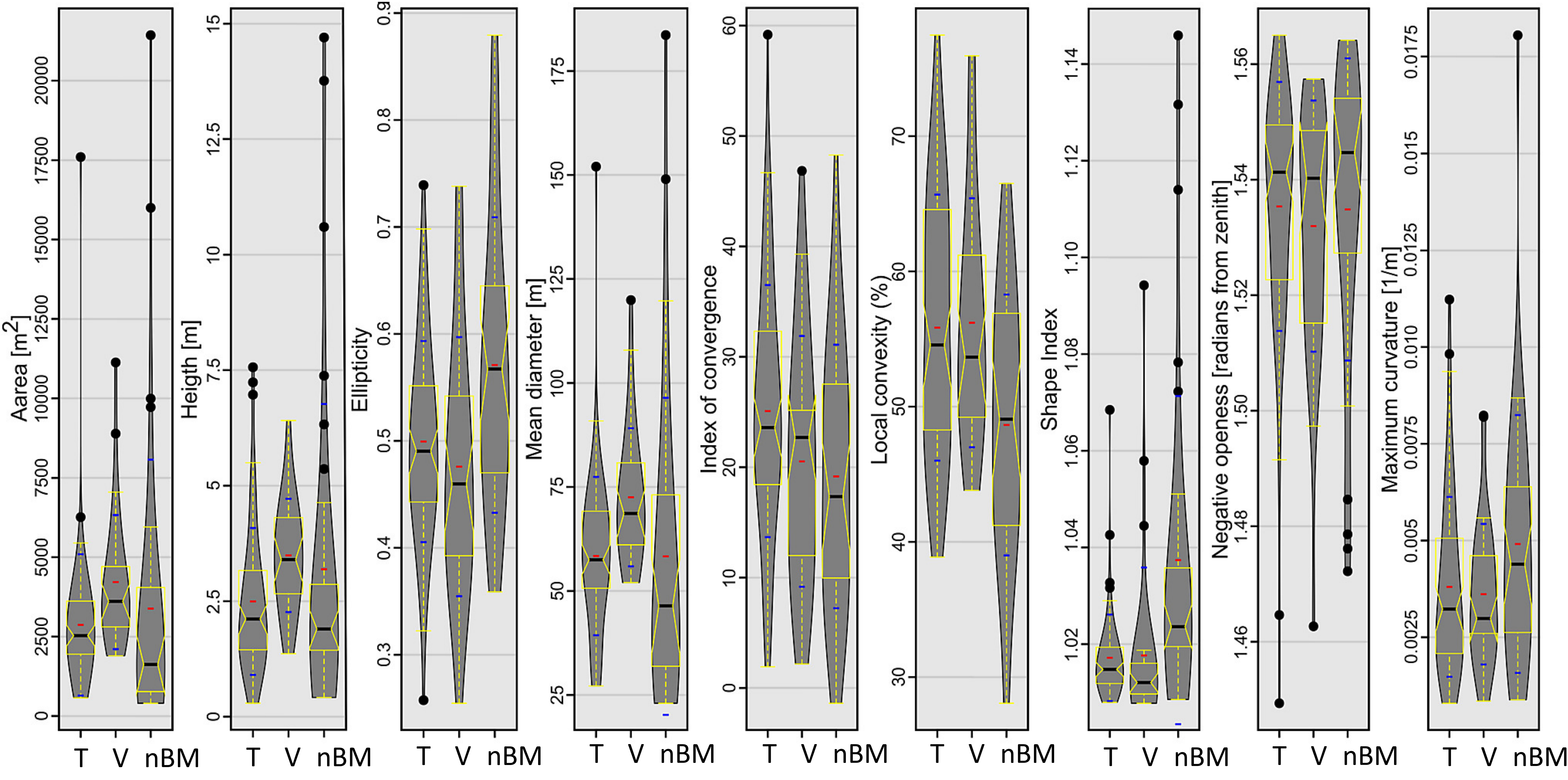

T – training BM [68] V – validation BM [29] nBM – mound of other type [33]

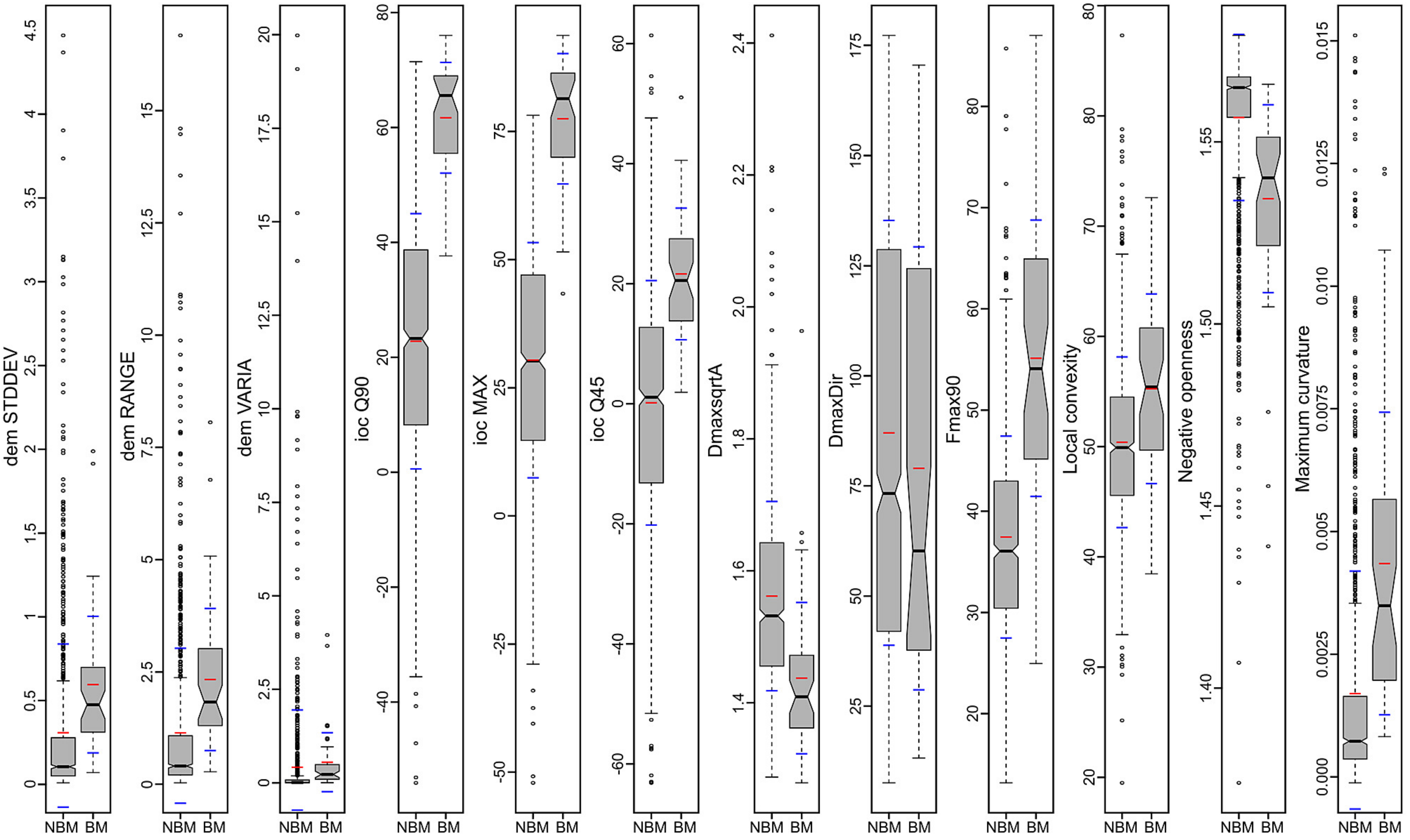
dem STDDEV
dem RANGE
dem VARIA
ioc Q90
ioc MAX
ioc Q45
DmaxsqrtA
DmaxDir
Fmax90
Local convexity
Negative openness
Maximum curvature
NBM
BM

Methodology – object based

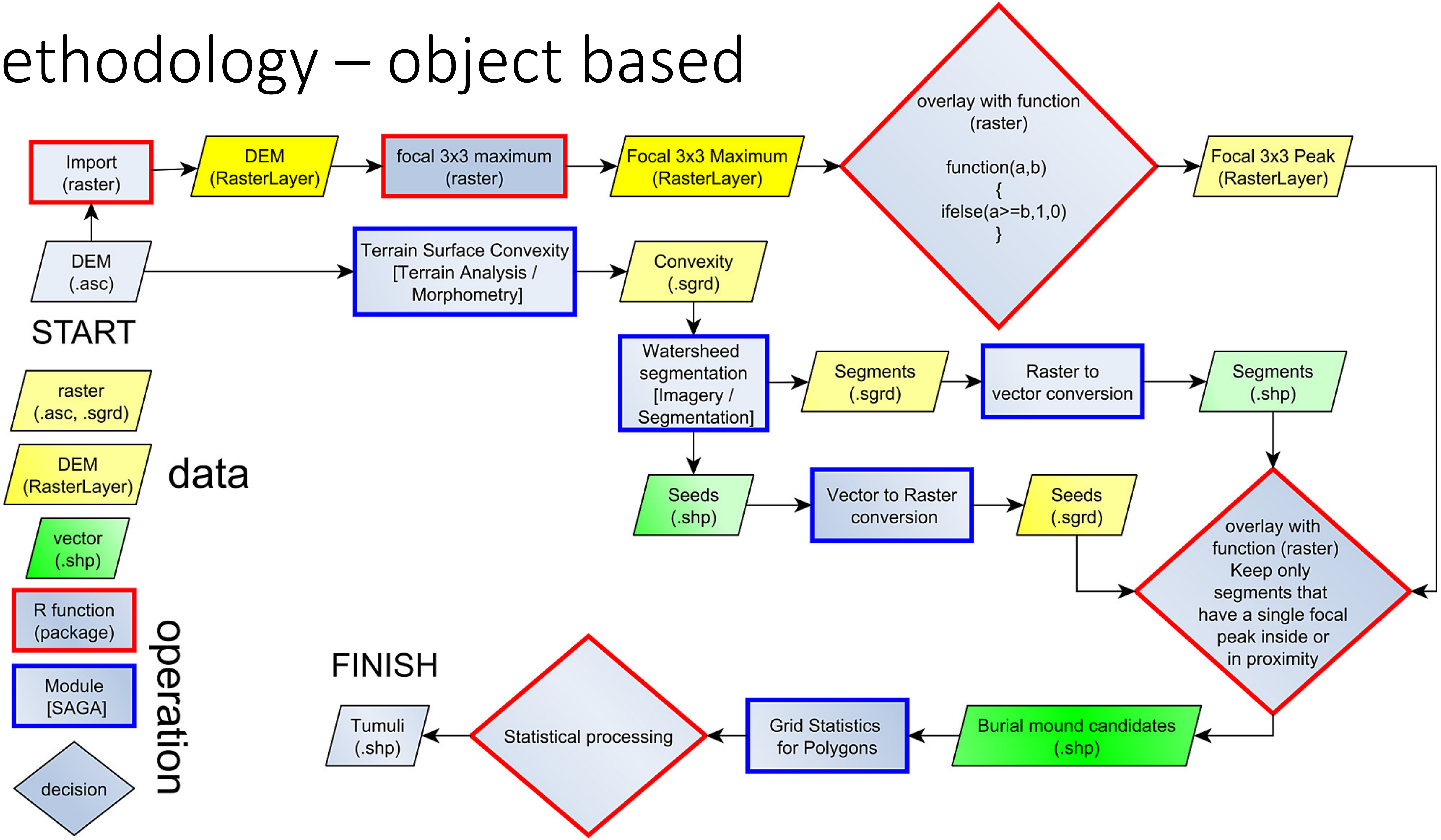

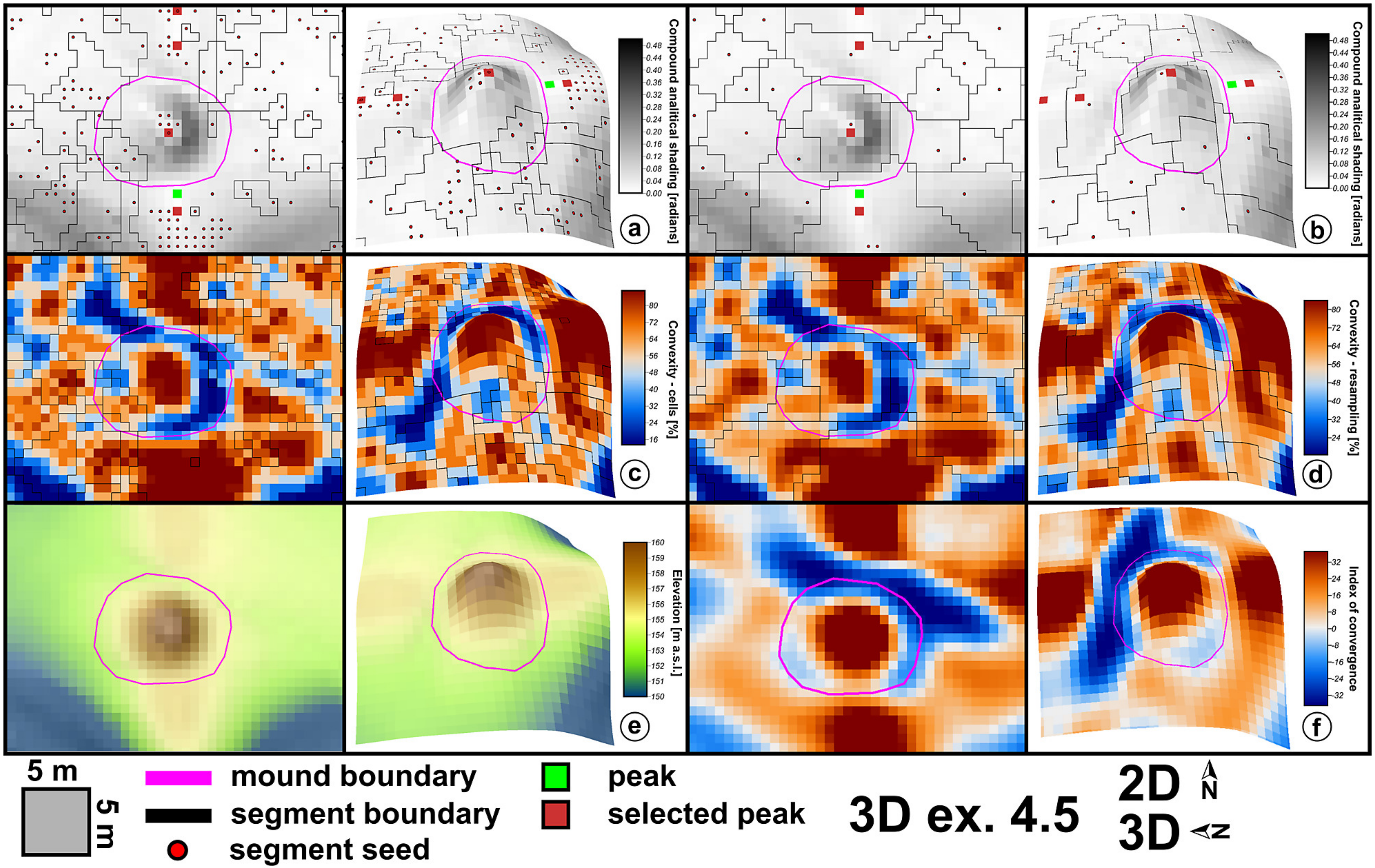

Compound analitical shading [radians]
0.48
0.44
0.40
0.36
0.32
0.28
0.24
0.20
0.16
0.12
0.08
0.04
0.00
a
b
Convexity - cells [%]
Convexity - resampling [%]
c
d
Elevation [m a.s.l.]
160
159
158
157
156
155
154
153
152
151
150
e
Index of convergence
f
5 m
5 m
mound boundary
segment boundary
segment seed
peak
selected peak
3D ex. 4.5
2D
N
3D
N

Local convexity (Iwahashi and Kamiya, 1995; Iwahashi and Pike, 2006)

- Percentage of convex-upward cells within a certain radius of pixels.
- It will include not only the peak as a maximum positive local relief but also the surrounding convex areas.
- This type of convexity is independent of relief magnitude.

During this step 2-3 tumuli are missed; they are mainly very flat tumuli, or degraded shape tumuli

- This parameter is ideal for the case of burial mounds, in terms of identifying the convexity of the burial mounds that is surrounded by flat or even convex areas.
- Nonetheless, by coupling the peak selection with local convexity gives the power of the method for selection the segments that are burial mound candidates.

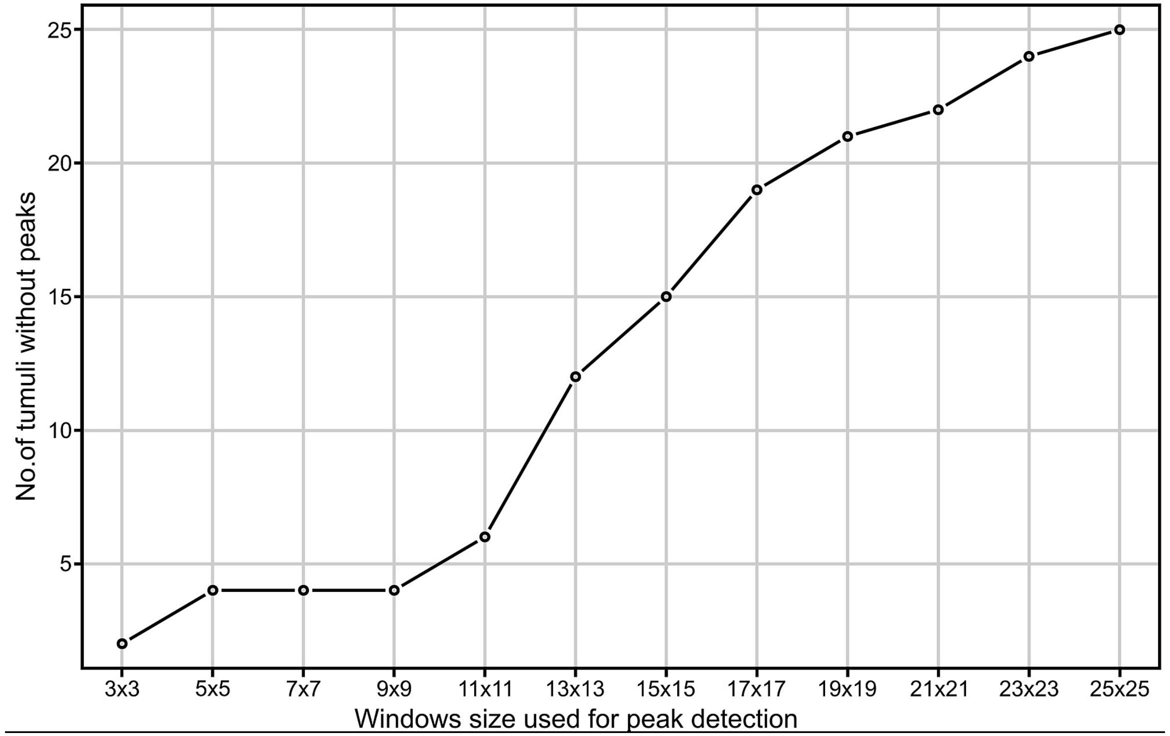

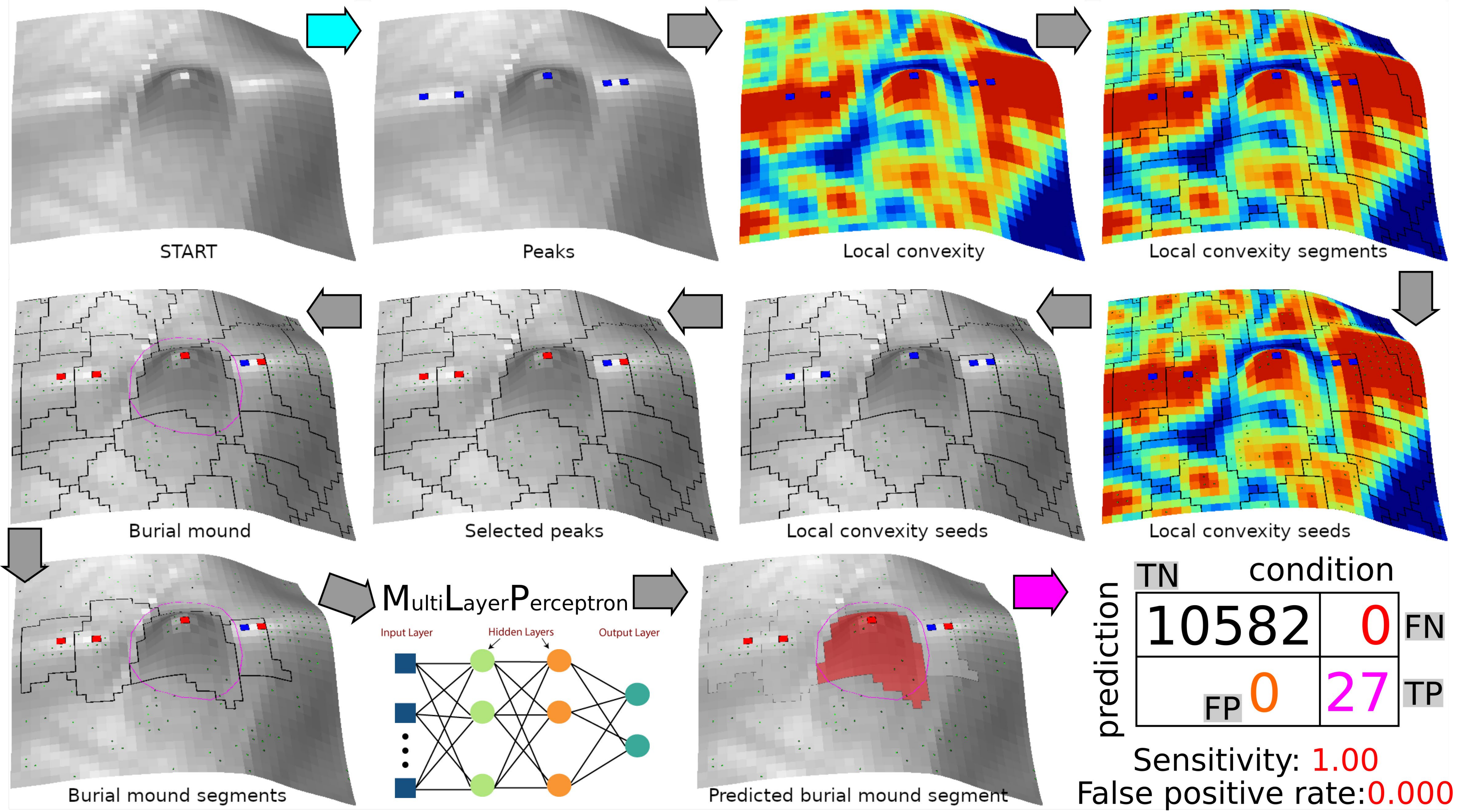
START
Peaks
Local convexity
Local convexity segments
Burial mound
Selected peaks
Local convexity seeds
Local convexity seeds
Burial mound segments
MultiLayerPerceptron
Input Layer
Hidden Layers
Output Layer
Predicted burial mound segment
TN
condition
prediction
10582
0
FN
FP
0
27
TP
Sensitivity: 1.00
False positive rate:0.000

Table S1. The list of geomorphometrical variables and their computation settings in SAGA GIS.

No	Code	Name	Description
1	A	Area	Polygon area
2	P	Perimeter	Polygon perimeter
3	P.A	Interior edge ratio	P/A
4	P.sqrt.A.		P/sqrt(A)
5	Depqc	Equivalent projected circle diameter	2*sqrt(A/π)
6	Sphericity	Sphericity	The ratio of the perimeter of the equivalent circle to the real perimter
7	Shape.Index	Shape index	Inverse of Sphericity
8	Dmax	Maximum diameter	Maximum distance between two polygon part's vertices
9	DmaxDir	Direction of maximum diameter	
10	Dmax.A	Dmax/A	
11	Dmax.sqrt.A	Dmax/sqrt(A)	
12	Dgyros	Diameter of gyration	Twice the maximum vertex distance to its polygon part's centroid
13	Fmax	Maximum Feret diameter	
14	FmaxDir	Direction of the maximum Ferret diameter	
15	Fmin	Minimum Feret diameter	
16	FminDir	Direction of the minimum Feret diameter	
17	Fmean	Mean Feret diameter	
18	Fmax90	Feret diameter measured at an angle of 90° to that of the Fmax direction	
19	Fmin90	Feret diameter measured at an angle of 90° to that of the Fmin direction	
20	Fvol	Diameter of a sphere having the same volume as the cylinder constructed by Fmin as the cylinder diameter and Fmax as its length	
21	dem	Elevation	
22	ioc	Index of convergence	
23	conv_r	Local convexity	
24	nego	Negative openness	
26	proc	Profile curvature	
27	plac	Plan curvature	
28	logc	Longitudinal curvature	
29	croc	Cross-sectional curvature	
30	minc	Minimum curvature	
31	maxc	Maximum curvature	
32	rare	Real surface area	
33	wind	Wind exposition index	
34	tpi	Topographic position index	
35	vld	Valley depth	
36	mpi	Morphometric protection index	
37	tri	Terrain ruggedness index	
38	vrm	Vector ruggedness measure	
39	txt	Terrain surface texture	
40	clo	Local curvature	
41	cup	Upslope curvature	
42	clu	Local upslope curvature	
43	cdo	Downslope curvature	
44	cdl	Local downslope curvature	
45	flo	Flow accumulation	
46	fpl	Flow path length	
47	spl	Slope length	
48	cbl	Cell balance	Ratio between flow input and output
49	twi	Topographic wetness index	SAGA implementation of TWI using a modified catchment area, that is more realistic, compared to standard TWi
51	dhratio	Diameter-height ratio	Dmax/dem RANGE
52	compactness	Compactness	(Sqrt(4*(A/π)))/P
53	formfactor	Form factor	(4*π*A)/(P/2)
54	roundness	Roundness	(4*A)/(π*Fmax)
55	elongation	Elongation	Fmax/Fmin

Table S2. The list of geomorphometrical variables and their computation settings in SAGA GIS.

No	Code	Name
1	A	Area
2	P	Perimeter
3	P.A	Interior edge ratio
4	P.sqrt.A.	
5	Depqc	Equivalent projected circle diameter
6	Sphericity	Sphericity
7	Shape.Index	Shape index
8	Dmax	Maximum diameter
9	DmaxDir	Direction of maximum diameter Dmax/A
10	Dmax.A	
11	Dmax.sqrt.A	
12	Dgyros	Diameter of gyration
13	Fmax	Maximum Feret diameter
14	FmaxDir	Direction of the maximum Ferret diameter
15	Fmin	Minimum Feret diameter
16	FminDir	Direction of the minimum Feret diameter
17	Fmean	Mean Feret diameter
18	Fmax90	Feret diameter measured at an angle of 90° to that of the Fmax direction
19	Fmin90	Feret diameter measured at an angle of 90° to that of the Fmin direction
20	Fvol	Diameter of a sphere having the same volume as the cylinder constructed by Fmin as the cylinder diameter and Fmax as its length
21	dem MIN	Minimum elevation
22	dem MAX	Maximum elevation
23	dem RANGE	Range of elevation
24	dem SUM	Sum of elevation
25	dem MEAN	Mean elevation
26	dem VARIAN	Elevation variance
27	dem STDDEV	Standard deviation of elevation
28	dem Q05	Elevation percentiles, multiples of 5
29	dem Q10	
30	dem Q15	
31	dem Q20	
32	dem Q25	
33	dem Q30	
34	dem Q35	
35	dem Q40	
36	dem Q45	
37	dem Q50	
38	dem Q55	
39	dem Q60	
40	dem Q65	
41	dem Q70	
42	dem Q75	
43	dem Q80	
44	dem Q85	
45	dem Q90	
46	dem Q95	
47	ioc MIN	Minimum index of convergence
48	ioc MAX	Maximum index of convergence
49	ioc RANGE	Range of index of convergence
51	ioc SUM	Sum of index of convergence
52	ioc MEAN	Mean index of convergence
53	ioc VARIAN	Index of convergence variance
54	ioc STDDEV	Standard deviation of index of convergence
55	ioc Q05	Indexs of confergence percentiles, multiples of 5
56	ioc Q10	
57	ioc Q15	
58	ioc Q20	
59	ioc Q25	
60	ioc Q30	
61	ioc Q35	
62	ioc Q40	
63	ioc Q45	
64	ioc Q50	
65	ioc Q55	
66	ioc Q60	
67	ioc Q65	
68	ioc Q70	
69	ioc Q75	
70	ioc Q80	
71	ioc Q85	
72	ioc Q90	
73	ioc Q95	

Multilayer Perceptron (MLP)

- Deep feedforward neural networks/multilayer perceptrons are methods that use the neuron model, of acyclic networks, in layers, that use connected functions as vector nodes to fit linear functions for an overall non-linear classification or regression.

Multi-layer Perceptron

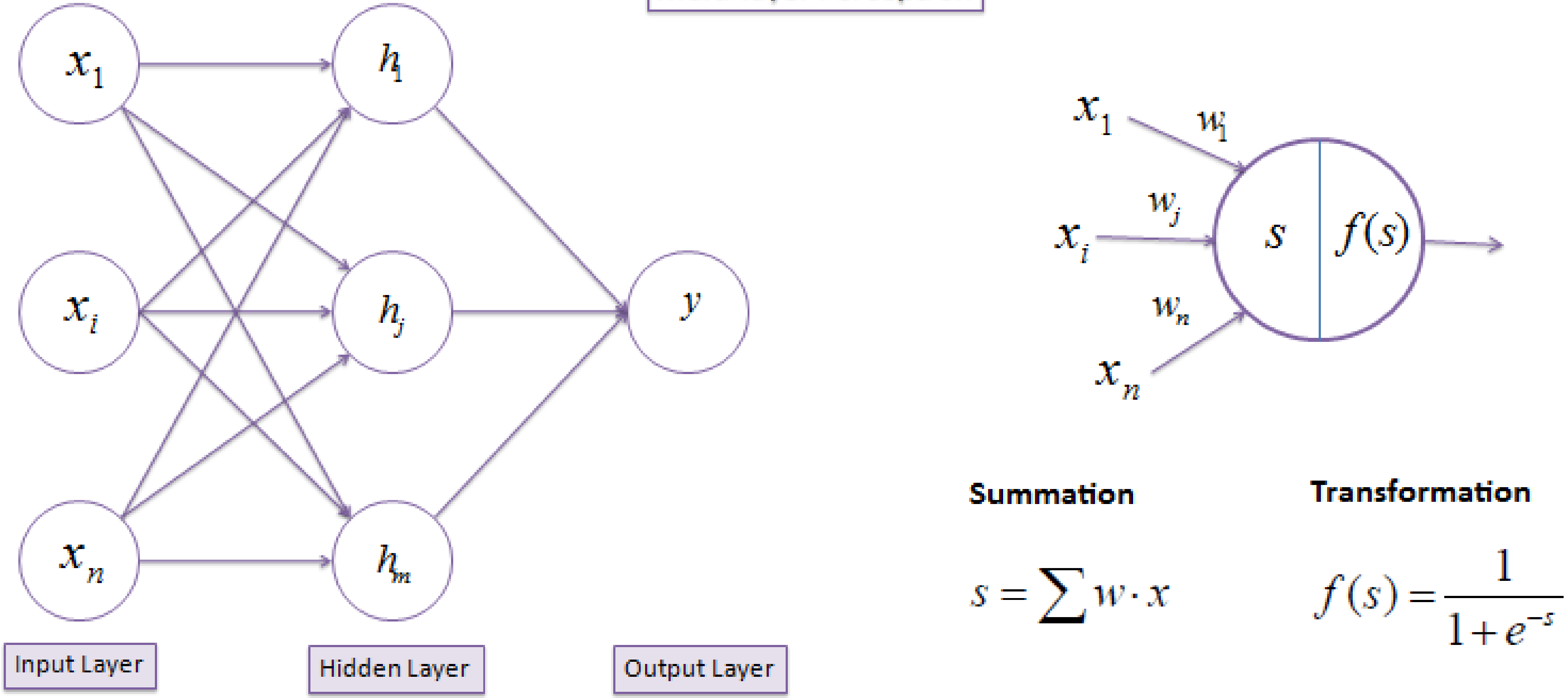

The learning curve is converging to 100% accuracy wery quickly – only after 15 epochs, for the training dataset (overfitting), but for the validation datasets 79 epoch are needed. At the 79 epoch the validation datasets reaches 100% accuracy.

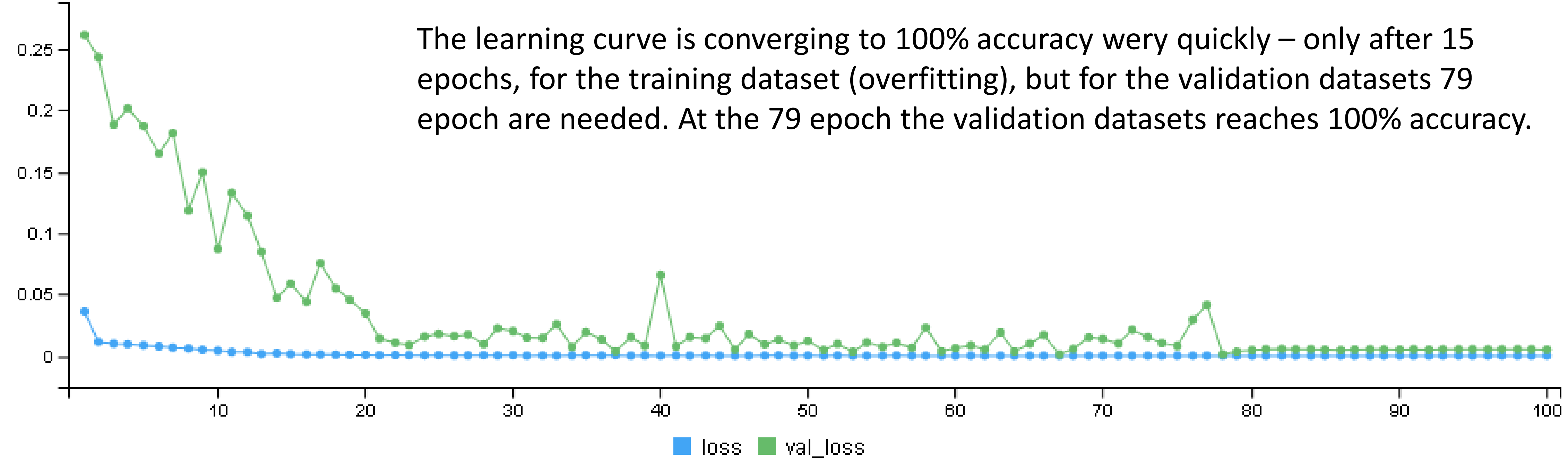

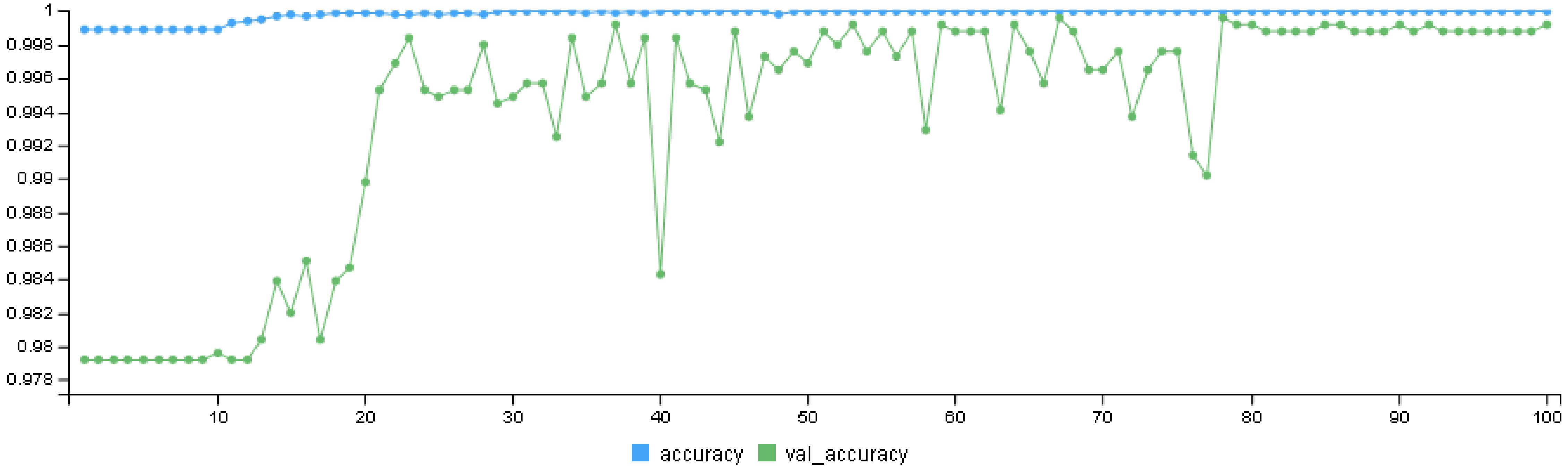

Deep MLP compared with the Random Forest

	RF/MLP parameters	TP	TN	FN	FP	SNS	FPR
TRAIN	1000 segments from which 75% burial mounds, 100 ntree, 5 mtry, 1 nodesize*	64	12 536	0	46	0.93	0.004
	Epochs 100 - train	62	12 681	2	0	0.99	0.000
TEST	1000 segments from which 75% burial mounds, 100 ntree, 5 mtry, 1 nodesize*	25	10 536	2	46	0.93	0.004
	Epochs 100 - test	27	10 582	0	0	1	0.000

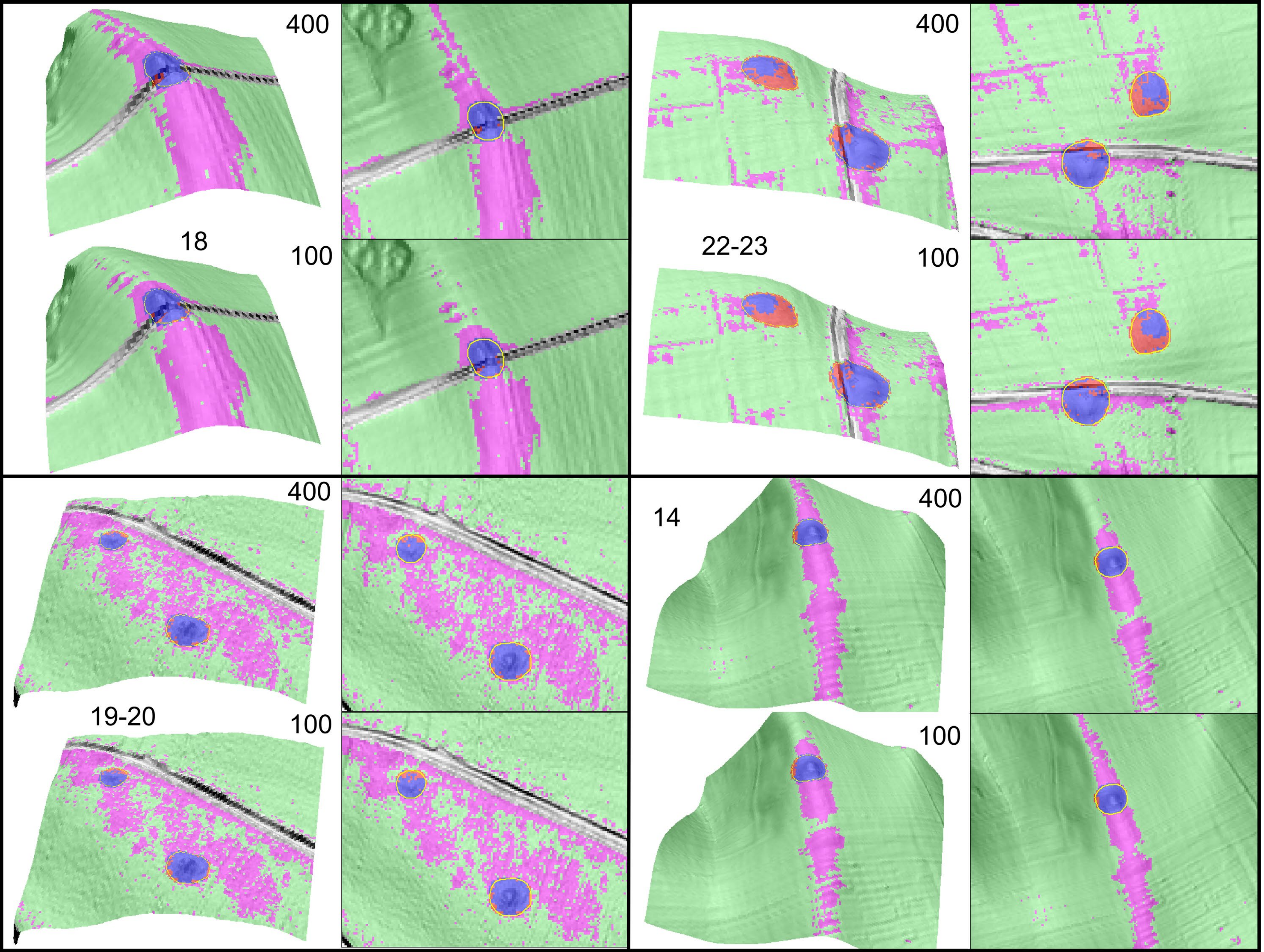

The RF parameters has impact mainly on the FP pixels.
Although the confusion matrix numeric variables might “look” better, actually the spatial representation is showing that wide areas are mapped as BM.

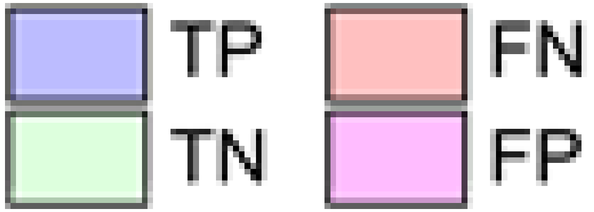

Sinkholes

concave features
5 m LiDAR DEM

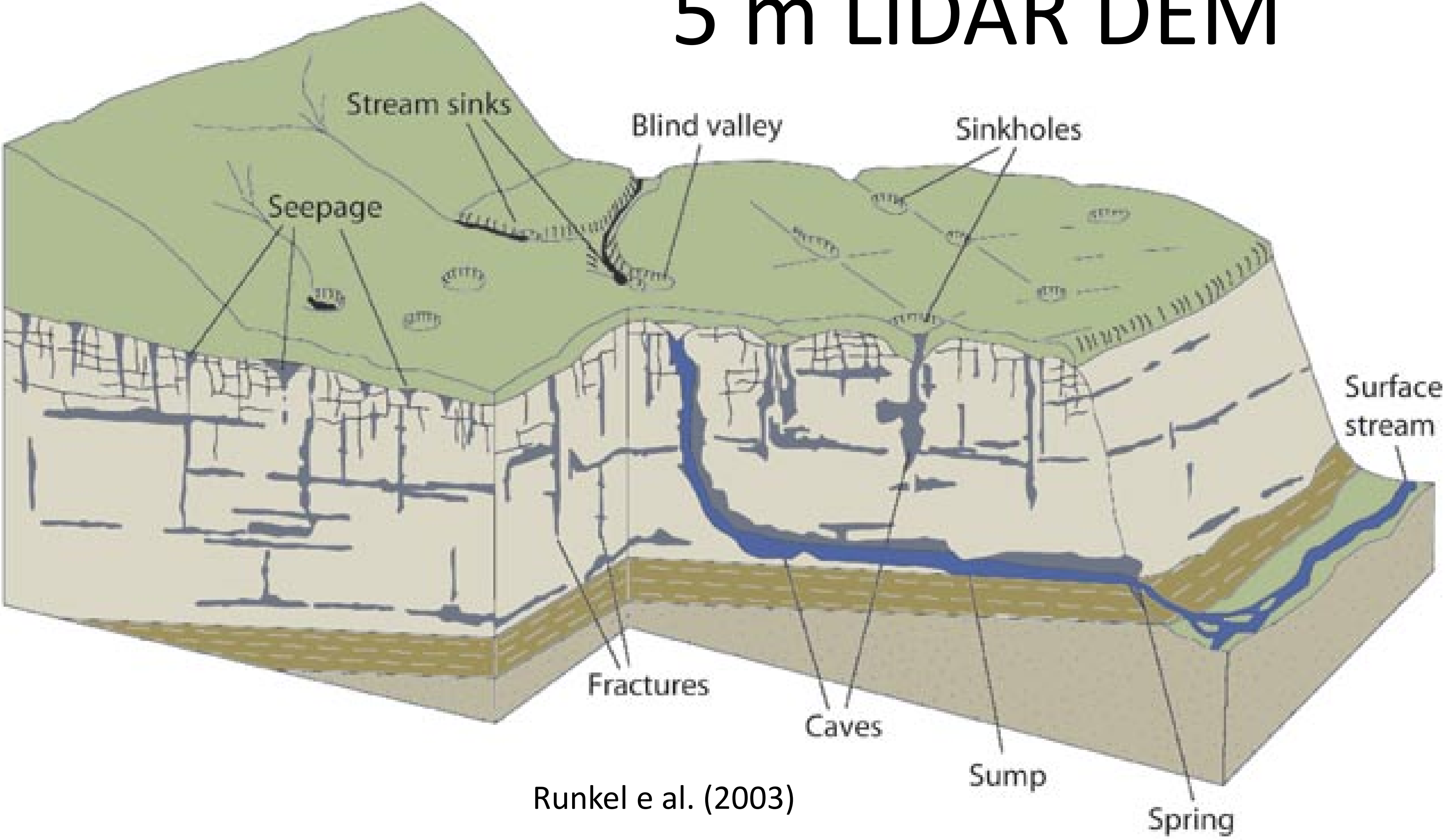

Runkel e al. (2003)

karstic

Watershed Segmentation of local concavity maxima

Adjacent Segments joined if the difference in seed value Bigger than 0.2

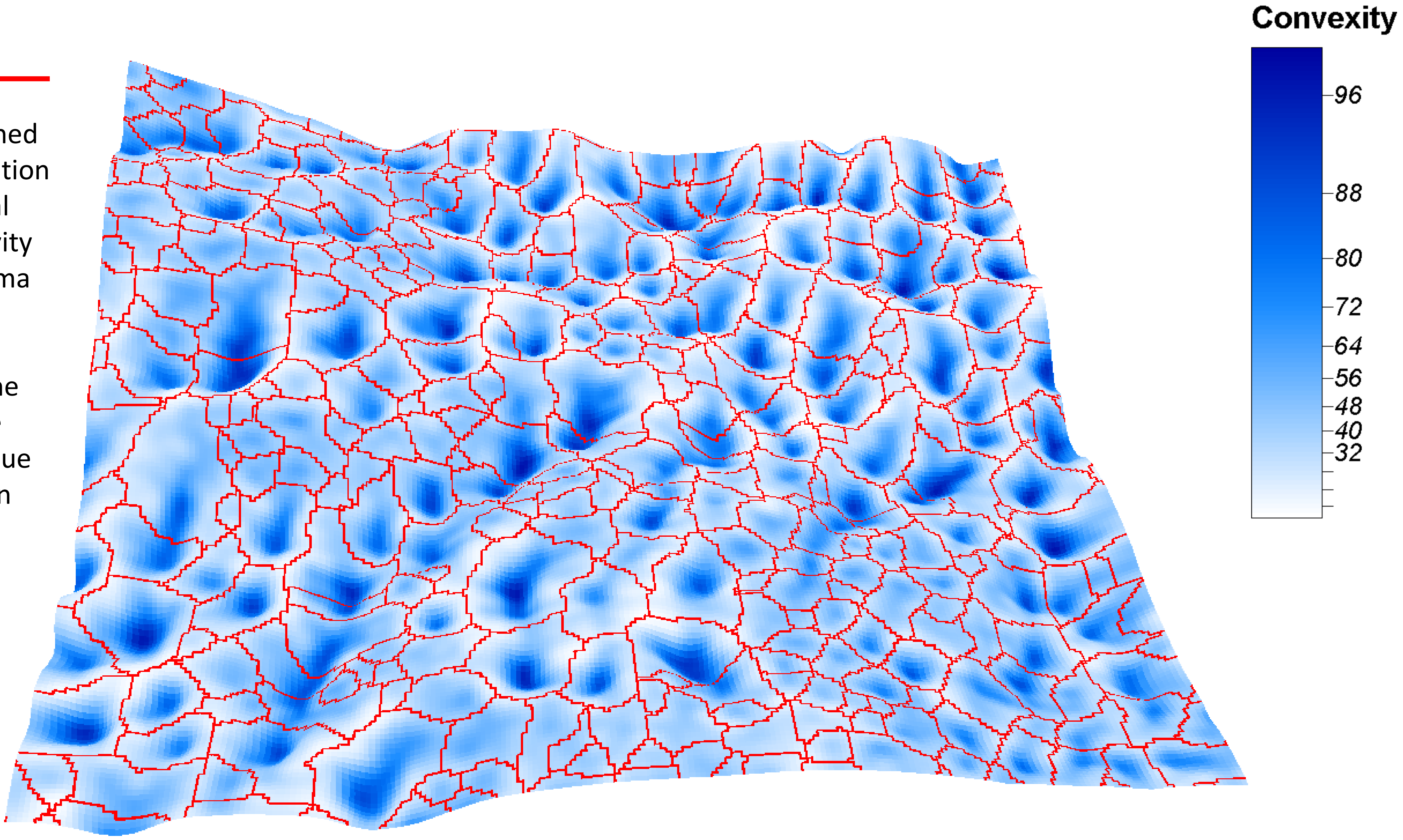

Watershed Segmentation of local concavity maxima

Adjacent Segments joined if the difference in seed value Bigger than 0.2

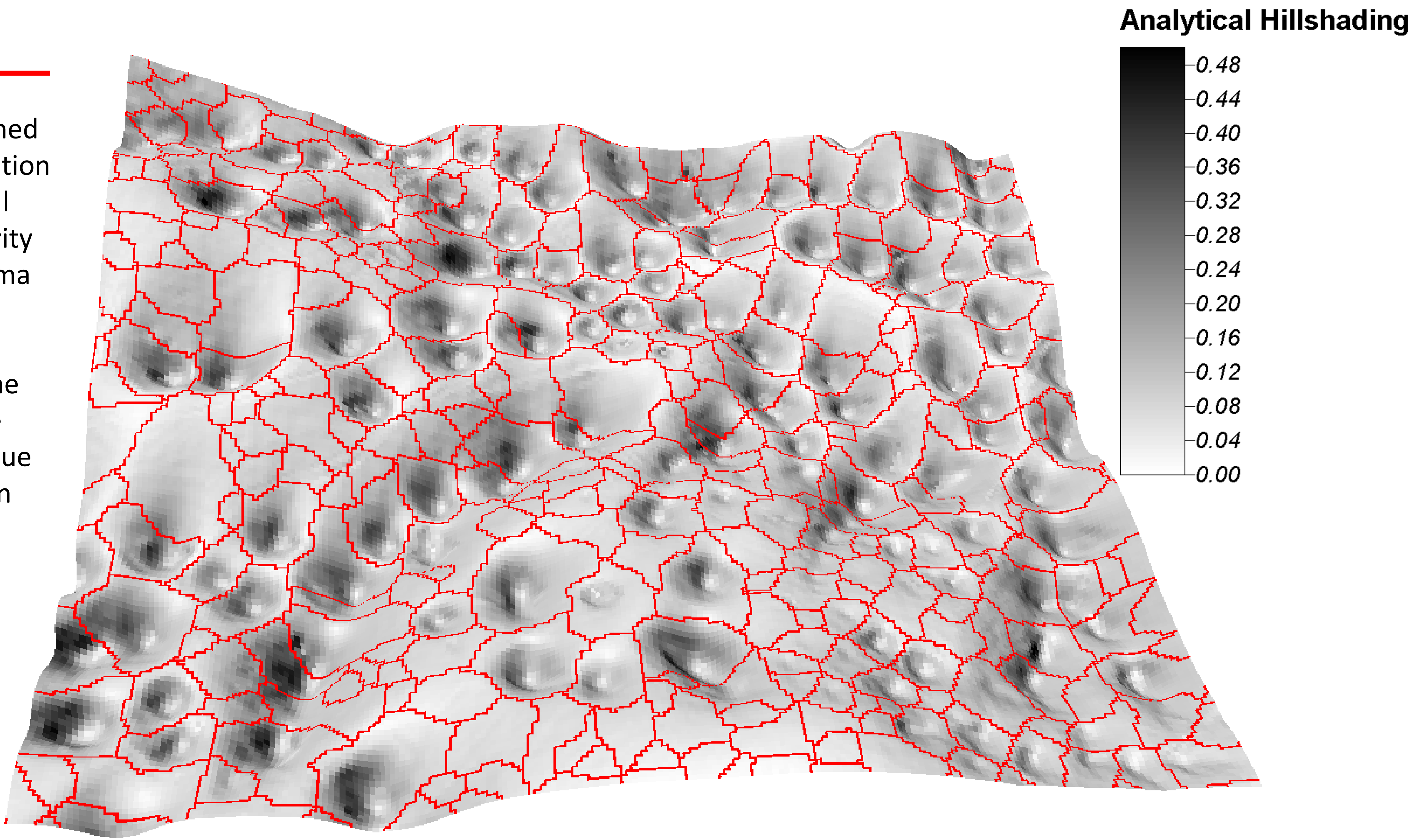

Pădurea Craiului Mts
Western Romania

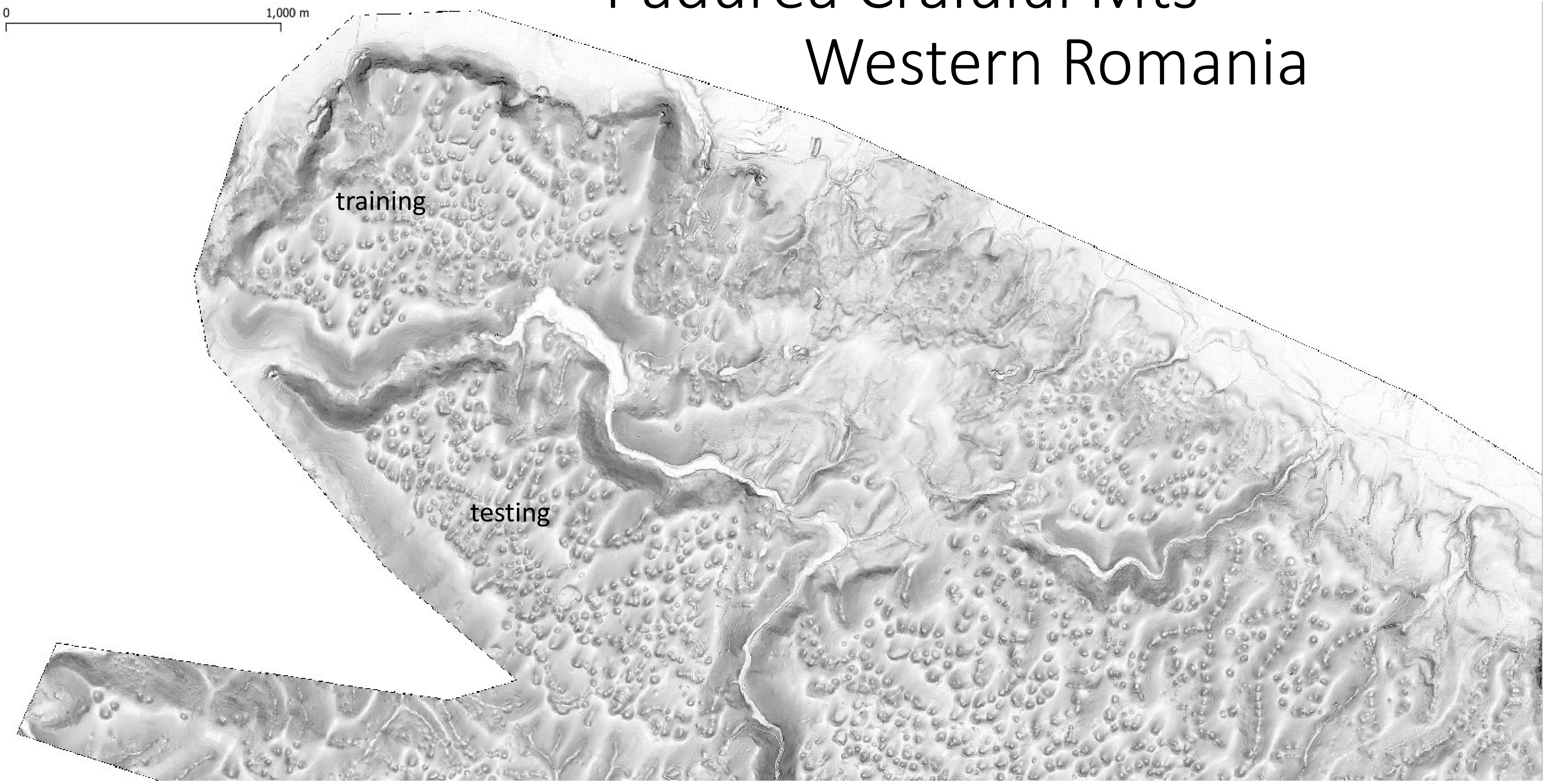

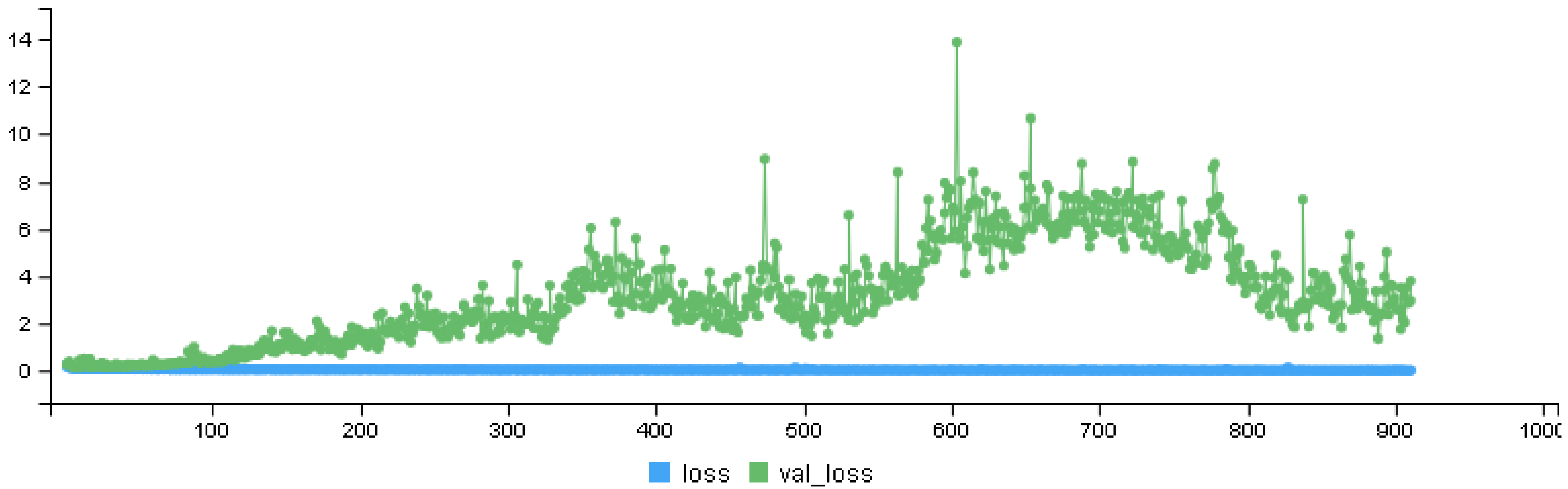

14
12
10
8
6
4
2
0
100
200
300
400
500
600
700
800
900
1000
loss
val_loss

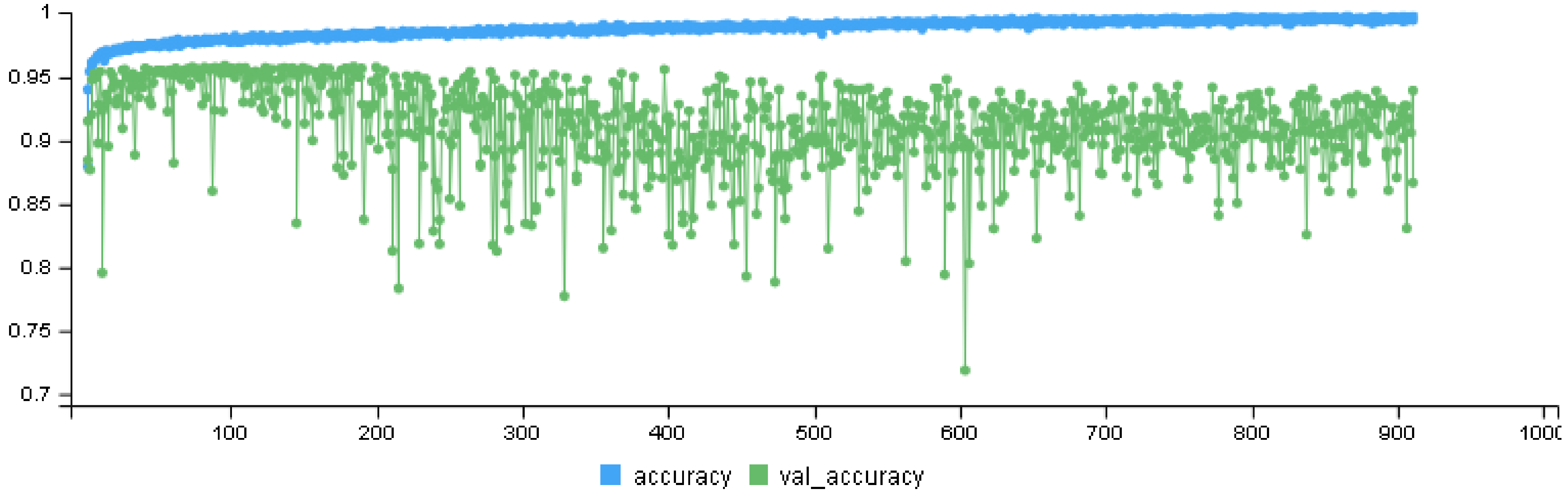

1
0.95
0.9
0.85
0.8
0.75
0.7
100
200
300
400
500
600
700
800
900
1000
accuracy
val_accuracy

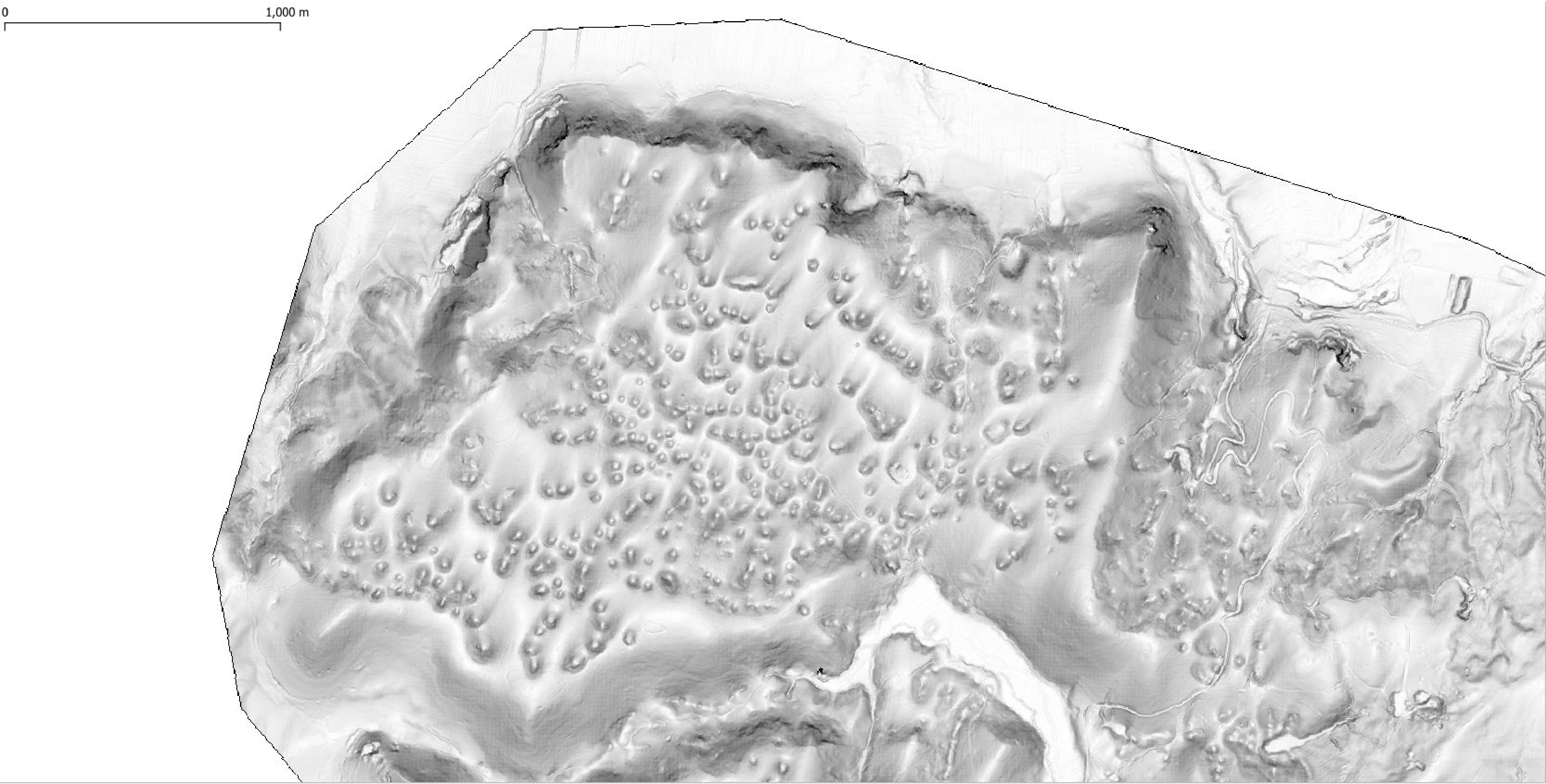
0
1,000 m

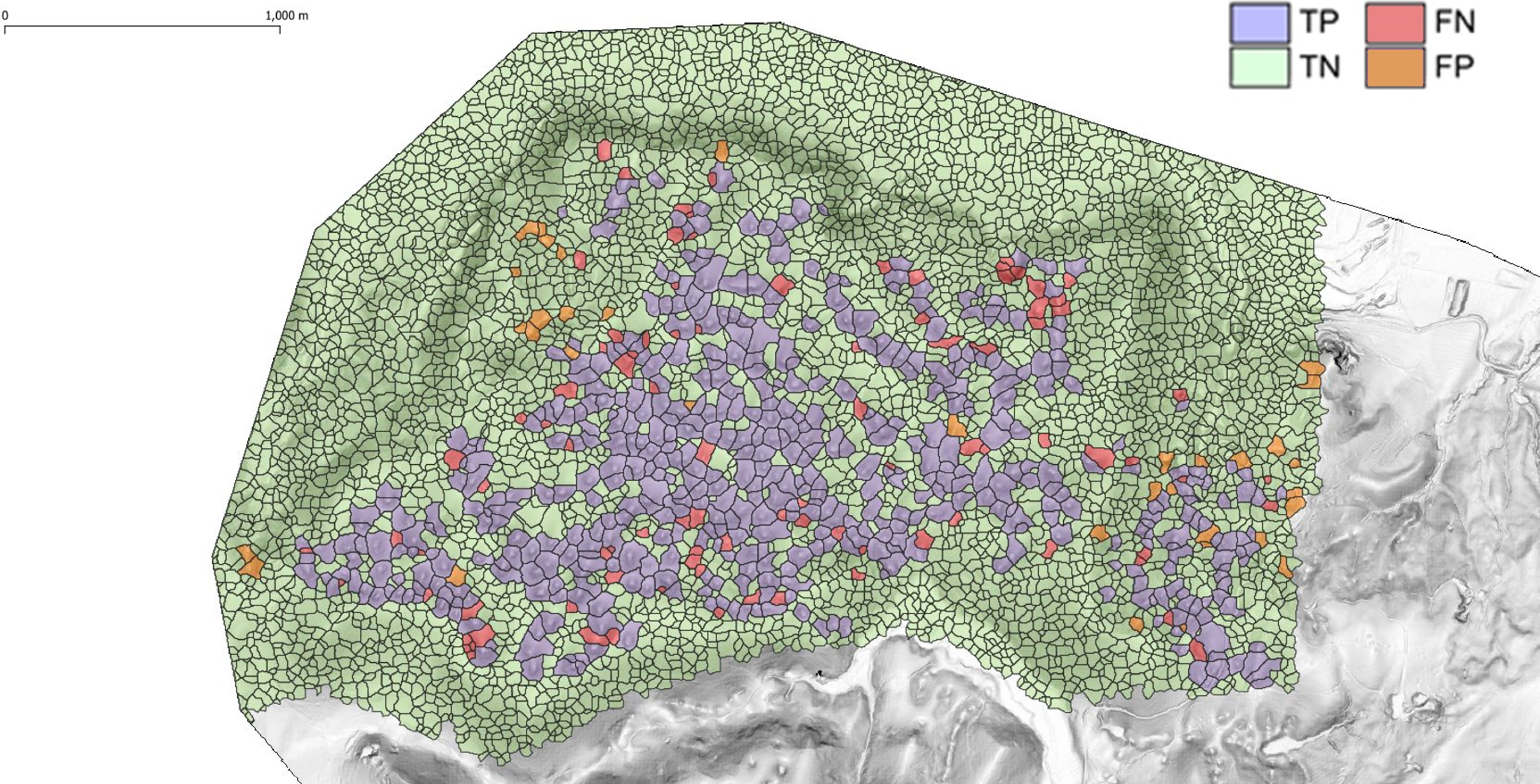
0
1,000 m
TP
FN
TN
FP


0
1,000 m

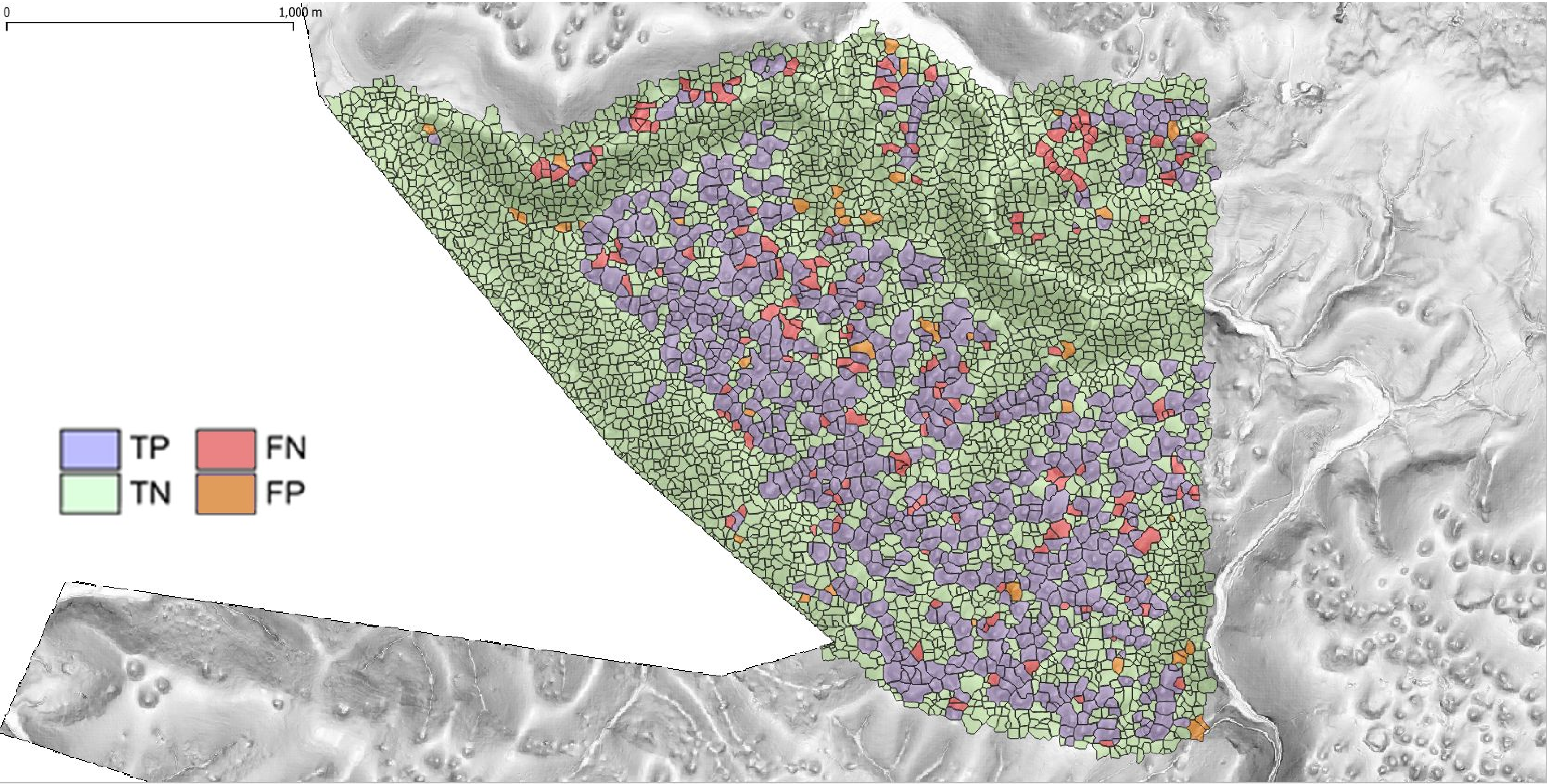
0
1,000 m
TP
FN
TN
FP

Train

Confusion Matrix and Statistics

Prediction	Reference 0	1
0	4663	93
1	35	508

Accuracy : 0.975844498962068
95% CI : (0.97134488155055, 0.979808918923813)
No Information Rate : 0.886582374032836
P-Value [Acc > NIR] : < 0.0000000000000002220446049250313

Kappa : 0.874611646088176

Mcnemar's Test P-Value : 0.0000005

Sensitivity : 0.99255002128565351
Specificity : 0.84525790349417640
Pos Pred Value : 0.98044575273338941
Neg Pred Value : 0.93554327808471482
Prevalence : 0.88658237403283635
Detection Rate : 0.87997735421777690
Detection Prevalence : 0.89752783544064918
Balanced Accuracy : 0.91890396238991490

Test

Confusion Matrix and Statistics

Prediction	Reference 0	1
0	3711	161
1	41	657

Accuracy : 0.955798687089715
95% CI : (0.949431994314811, 0.961574310375017)
No Information Rate : 0.821006564551422
P-Value [Acc > NIR] : < 0.0000000000000002220446049250313

Kappa : 0.840458111310513

Mcnemar's Test P-Value : < 0.0000000000000021

Sensitivity : 0.98907249466950964
Specificity : 0.80317848410757942
Pos Pred Value : 0.95841942148760328
Neg Pred Value : 0.94126074498567358
Prevalence : 0.82100656455142229
Detection Rate : 0.81203501094091901
Detection Prevalence : 0.84726477024070024
Balanced Accuracy : 0.89612548938854453

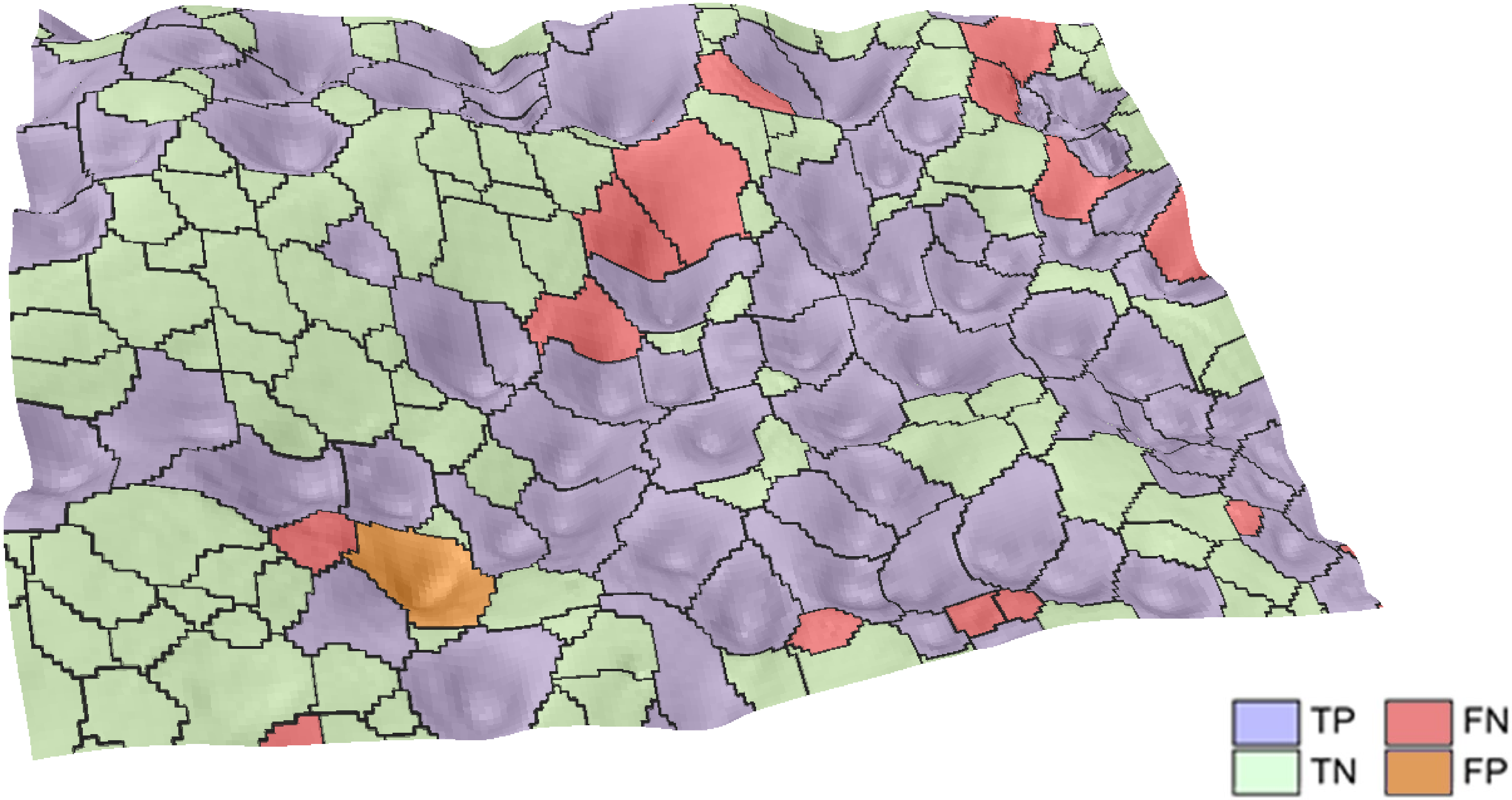
TP
FN
TN
FP

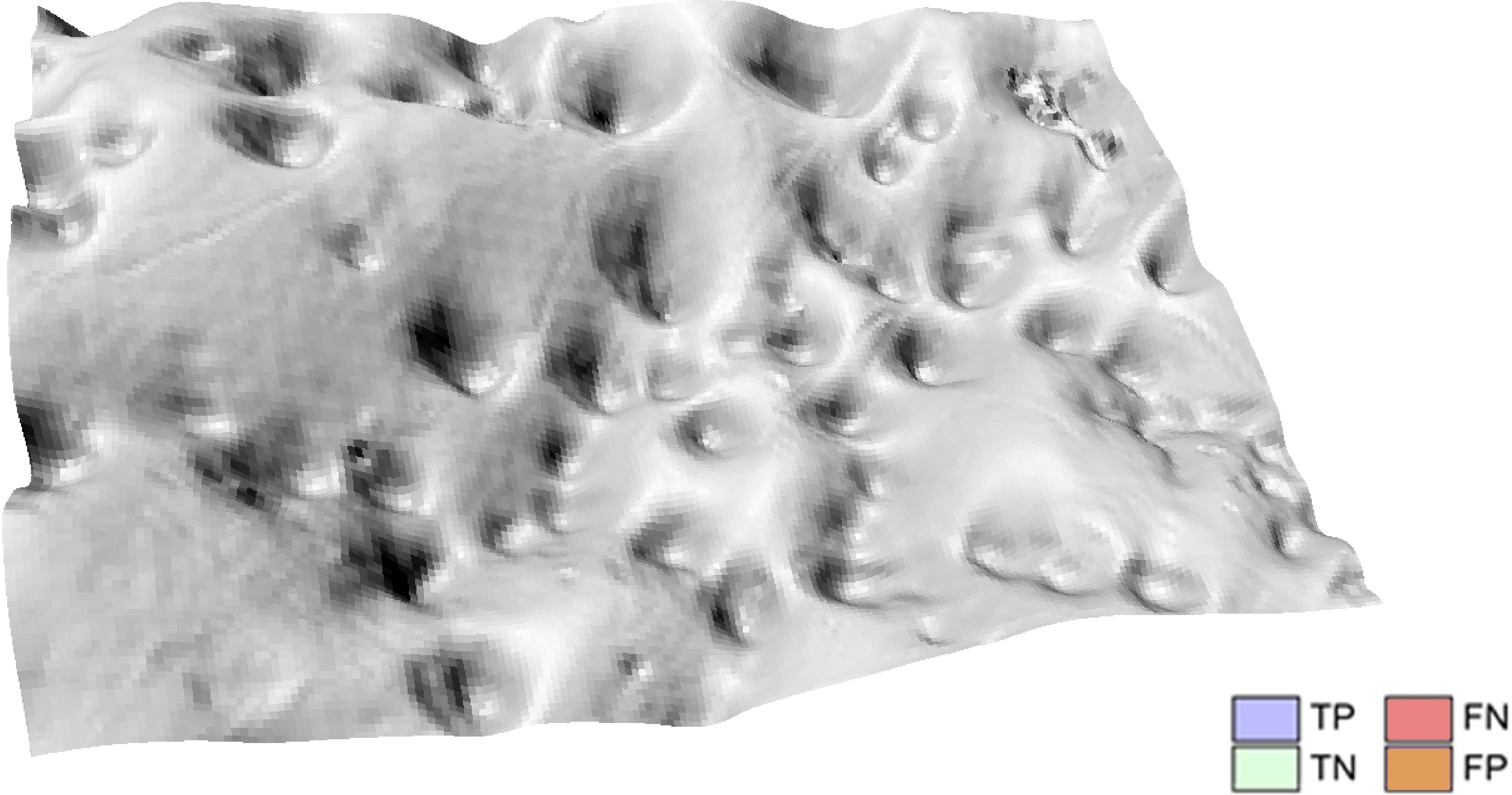
TP
FN
TN
FP

Conclusions

- I have shown that the MLP is able to train models that detect convex and concave features, with good generalisation.
- The segmentation is a powerfull tool that reduce the complexity of the task.
- Analysing the correlation matrix the main issue remaining for the sinkholes is the accuracy of the segmentation.
- Anyway while this can be improved, the Stepinski approach of segmentation followed by classification I think is the best approach in landform classification approaches.
- By adding the power of the ML & AI this workflow should be extended to include neighbourhood information, to be able to classify compound shapes.

Thank you for your attention!

- Niculiță M (2020) Geomorphometric Methods for Burial Mound Recognition and Extraction from High-Resolution LiDAR DEMs, Sensors, https://www.mdpi.com/1424-8220/20/4/1192/htm
- Niculiță M (2020) Burial mound detection using geomorphometry and statistical methods pixels versus objects, in Massimiliano Alvioli, Ivan Marchesini, Laura Melelli, and Peter Guth, Proceedings of the Geomorphometry 2020 Conference, Perugia, Italy, CNR Edizioni, 26-29, DOI: 10.30437/geomorphometry2020_7